

This is an Open Access document downloaded from ORCA, Cardiff University's institutional repository: <https://orca.cardiff.ac.uk/id/eprint/120634/>

This is the author's version of a work that was submitted to / accepted for publication.

Citation for final published version:

Qi, Shuai, Cui, Yu-Jun, Chen, Ren-Peng, Wang, Hanlin, Lamas-Lopez, Francisco, Aïmedieu, Patrick, Dupla, Jean-Claude, Canou, Jean and Saussine, Gilles 2019. Influence of grain size distribution of inclusions on the mechanical behaviors of track-bed materials. *Géotechnique* 10.1680/jgeot.18.p.047

Publishers page: <http://dx.doi.org/10.1680/jgeot.18.p.047>

Please note:

Changes made as a result of publishing processes such as copy-editing, formatting and page numbers may not be reflected in this version. For the definitive version of this publication, please refer to the published source. You are advised to consult the publisher's version if you wish to cite this paper.

This version is being made available in accordance with publisher policies. See <http://orca.cf.ac.uk/policies.html> for usage policies. Copyright and moral rights for publications made available in ORCA are retained by the copyright holders.



Accepted manuscript doi: 10.1680/jgeot.18.p.047

Accepted manuscript

As a service to our authors and readers, we are putting peer-reviewed accepted manuscripts (AM) online, in the Ahead of Print section of each journal web page, shortly after acceptance.

Disclaimer

The AM is yet to be copyedited and formatted in journal house style but can still be read and referenced by quoting its unique reference number, the digital object identifier (DOI). Once the AM has been typeset, an 'uncorrected proof' PDF will replace the 'accepted manuscript' PDF. These formatted articles may still be corrected by the authors. During the Production process, errors may be discovered which could affect the content, and all legal disclaimers that apply to the journal relate to these versions also.

Version of record

The final edited article will be published in PDF and HTML and will contain all author corrections and is considered the version of record. Authors wishing to reference an article published Ahead of Print should quote its DOI. When an issue becomes available, queuing Ahead of Print articles will move to that issue's Table of Contents. When the article is published in a journal issue, the full reference should be cited in addition to the DOI.

Accepted manuscript doi: 10.1680/jgeot.18.p.047

Submitted: 25 February 2018

Published online in ‘accepted manuscript’ format: 21 February 2019

Manuscript title: Influence of Grain Size Distribution of Inclusions on the Mechanical Behaviors of Track-bed Materials

Authors: Shuai Qi^{*,†}, Yu-Jun Cui[†], Ren-Peng Chen^{*}, Han-Lin Wang^{*,†}, Francisco Lamas-Lopez[†], Patrick Aïmediou[‡], Jean-Claude Dupla[†], Jean Canou[†] and Gilles Saussine[§]

Affiliations: ^{*}Zhejiang University, China; [†]Laboratoire Navier/CERMES, Ecole des Ponts ParisTech (ENPC), France; [‡]Laboratoire Navier, UMR 8205, ENPC, IFSTTAR, CNRS, UPE, France and [§]Société Nationale des Chemins de Fer (SNCF), France

Corresponding author: Yu-Jun Cui, Ecole des Ponts ParisTech, 6-8 av. Blaise Pascal, Cité Descartes, Champs-sur-Marne, F-77455 Marne La Vallée – France. Tel.: +33 1 64 15 35 50.

E-mail: yu-jun.cui@enpc.fr

Abstract

In the French conventional railway track-bed, an interlayer was created, mainly from the interpenetration of ballast and subgrade. Field investigation showed that the ballast content decreases over depth. In addition, depending on the locations the grain size distribution of ballast grains can be quite different, defining different values of coefficient of uniformity C_u . In this study, triaxial tests were carried out on the interlayer soil with 3 C_u values and 5 volumetric inclusion contents f_v . X-ray μ CT scans were also conducted on representative samples to visualize the corresponding inclusion distributions. Results show that i) at all 3 C_u values, two soil fabrics can be identified, namely grain-grain contact structure for large inclusion contents ($f_v = 35\%$ and 45%) and fine-fine contact structure for small inclusion contents ($f_v = 5\%$, 10% and 20%), and the characteristic volumetric inclusion content f_{v-cha} separating these two categories was larger for smaller C_u since in this case less inclusion contacts were expected to be developed at a given f_v ; ii) for the grain-grain contact structure, a smaller C_u caused larger maximum deviator stress q_{max} , larger friction angle, larger Poisson's ratio and more dilatancy due to the involvement of more large grains at smaller C_u ; iii) for the fine-fine contact structure, an opposite trend was observed: the smaller the C_u , the smaller the q_{max} the friction angle, the Poisson's ratio and the dilatancy due to the less quantity of inclusion grains; iv) the change patterns of Young's modulus and cohesion with increasing C_u were the same for the two soil fabrics - Young's modulus and cohesion decreased with the increase of C_u .

Keywords: fabric/structure of soils; gravels; laboratory tests; particle-scale behaviour; shear strength; deformation

Introduction

In France, 94% of the total railway network is constituted by the ancient railway lines, which were built by directly placing the ballast onto the subgrade without separation layer between them. Under years of traffic loadings, a layer namely interlayer was formed, mainly through the interpenetration of fines and ballast. According to the in-situ investigation (Trinh 2011), the content of inclusions (ballast grains) decreases over depth, and roughly two distinct soil fabrics are identified: a ballast grain skeleton with fine particles contained in the pores of grain skeleton for the upper part and a fine matrix with ballast grains floating in it for the lower part. In the French program of conventional railway lines renewal, this interlayer with a dry unit mass as high as 2.4 Mg/m^3 (Trinh 2011) was maintained due to its favorable mechanical behavior. Thus, a series of studies have been conducted, especially on the upper part of the interlayer, aiming to clarify the effect of fines and water contents on the mechanical behavior by both monotonic and cyclic triaxial tests (Trinh et al. 2012; Cui et al. 2013; Duong et al. 2013; Duong et al. 2016; Lamas-Lopez 2016). The results showed that the increase of water content decreased the shear strength and enlarged the permanent deformation. In addition, the effect of fines content was closely related to the degree of saturation of the interlayer: when the interlayer was in saturated state, adding fines increased the permanent deformation and decreased the resilient modulus, whereas opposite changes occurred in unsaturated state. Moreover, the static and dynamic responses of the interlayer with different inclusion contents were also studied (Wang et al. 2017, Wang et al. 2018a,

Wang et al. 2018b). The results showed that there was a characteristic volumetric inclusion content $f_{v\text{-cha}}$; the shear strength and dynamic properties (resilient modulus; damping ratio) changed slightly when $f_v < f_{v\text{-cha}}$ and this change became significant when $f_v > f_{v\text{-cha}}$. The $f_{v\text{-cha}}$ corresponded to the transition of soil fabrics from a grain dominated skeleton to a fine dominated skeleton.

Because the interlayer is naturally formed at different locations along the railway lines, the grain size distribution of the inclusions characterized by $C_u = d_{60}/d_{10}$ (Coefficient of Uniformity) inevitably varies. As a result, the mechanical behavior of the interlayer soils can change. From a practical point of view, this aspect needs to be studied in depth. Numerous studies were undertaken, dealing with the effect of C_u on the mechanical behavior of sands in terms of small strain shear modulus, shear strength, etc. (Menq 2003; Kokusho et al. 2004; Igwe et al. 2007; Wichtmann and Triantafyllidis 2009; Monkul et al. 2016). To date, the results obtained have not been conclusive. Moreover, to the authors' knowledge, there are a few studies focusing on soils containing coarse grains. Seif EI Dine et al. (2010) studied a soil mixture of sand and coarse grains at two volumetric inclusion contents and reported that more uniform inclusions with smaller C_u value led to larger maximum deviator stress and more significant dilatancy. Their work was limited to one kind of soil fabric in which coarse inclusions were not in contact with each other. Moreover, the matrix was constituted of a cohesionless soil – a sand, which does not represent the case of interlayer soils which involve a large amount of fine-grained soils.

In this study, the mechanical behaviors of a soil mixture were investigated with 3 C_u values at 5 inclusion contents by conducting monotonic triaxial tests. The fines part of the mixture was prepared by simulating the fines of “Sénissiat site” (Trinh et al. 2011) in terms of grain size distribution and plasticity index. The coarse inclusions were prepared by applying a similitude method (Lowe 1964) based on the grain size distribution curve of real ballast. This method of materials preparation allowed overcoming the difficulty in taking natural interlayer soils on the one hand, and avoiding to use large-scale experimental devices on the other hand. The samples were prepared by dynamic compaction and the fines in all samples were kept at the optimum water content and the maximum dry density. X-ray μ CT scans were performed to identify the structure of soils, in particular the distribution of coarse inclusions inside the soil samples. It is worth noting that this experimental study was limited to triaxial tests on scaled-down ballast inclusions mixed with one soil and at a single water content. Thus, the results obtained cannot be directly generalised to predict/analyse the interlayer mechanical behaviour in the field complex conditions. However, they can greatly help well understand the mechanisms related to the effects of C_u at different inclusion contents.

Materials and methods

Materials

Since obtaining large quantity of in-situ interlayer soils was difficult, fines and inclusions constituting such soils were fabricated in the laboratory. The fines part was prepared

following a method proposed by Lamas-Lopez (2016) and used later by Wang et al. (2018a) to simulate the case of “Sénissiat site” (Trinh 2011). In this method, nine commercial soils were mixed together with the mass proportions calculated according to the target grain size distribution (see Table 1). The grain size distribution of the fabricated fines (Fig. 1), along with the liquid limit $w_L = 32.0\%$ and plasticity index $I_p = 20\%$, agreed well with those of the in-situ ones (Wang et al. 2018a).

The maximum ballast grain diameter at “Sénissiat site” (Trinh 2011) can reach 63 mm (Fig. 2). Since the diameter of the sample should be larger than 5 times the maximum grain diameter to minimize the sample size effect (Fagnoul and Bonnechere 1969; Nitchiporovitch 1969; Trinh et al. 2012; Duong et al. 2013; Lamas-Lopez 2016; Wang et al. 2018a), in order to use a triaxial cell of 100 mm diameter, micro-ballast with a maximum grain size $d_{max} = 20$ mm (Fig. 2) and with a grain size distribution curve determined through the similitude method (Lowe 1964) was used. Details about this method can be found in Wang et al. (2018a). To prepare the micro-ballast, three kinds of commercial soils (G10-20, G4-10 and HN2-4) were mixed. Their grains size distributions were also shown in Fig. 2.

The above-mentioned micro-ballast fabricated by Wang et al. (2018a) was termed as S1 and the corresponding experimental results were taken for comparison in this study. In order to study the effect of C_u of inclusions, other two inclusions termed as S2 and S3 were designed and fabricated by reducing the proportion of the smaller grains as compared with S1. For S2, soil HN2-4 was not employed and the fraction of G4-10 was decreased. For S3,

only soil grains from G10-20 with sizes ranging from 16 mm to 20 mm were used after removing the grains smaller than 16 mm by sieving. Table 2 compares the proportions of the soils constituting S1, S2 and S3. The designed grain size distributions of S1, S2 and S3 were put together and represented in Fig.3, with their designed C_u values equal to 2.72, 2.01 and 1.12, respectively. As can be seen from Fig. 3, a smaller C_u value corresponded to a steeper curve and a narrow grain size range, indicating a more uniform pattern. Fig. 3 compares the measured and calculated grain size distributions of S1, S2 and S3. A good agreement can be observed.

Methods

To characterize the amount of inclusions in a sample, a parameter namely volumetric inclusion content f_v (Pedro 2004; Seif El Dine et al. 2010; Wang et al. 2017) was adopted:

$$f_v = V_{in} / V_{total} \quad (1)$$

where V_{in} and V_{total} are the total inclusion volume and the total sample volume, respectively.

The total sample volume V_{total} consists of two parts: the inclusion volume V_{in} and the fines volume V_{fines} . The inclusion volume V_{in} corresponds to the volume of the solid micro-ballast grains without pores voids. All pores are assumed to be contained in the fines volume V_{fines} .

The f_v value of the natural interlayer soils at “Sénissiat site” (Trinh 2011) was 52.9%. In this study, five f_v values (namely, 5%, 10%, 20%, 35%, 45%) and three C_u values (2.72, 2.01 and 1.12) were considered. Note that the case of $C_u = 2.72$ was already studied by Wang et al. (2018a). For a given f_v , the inclusion volume V_{in} and the fines volume $V_{fines} = V_{total} - V_{in}$ can be easily determined when the total sample volume is known. Then, the total mass of the

inclusions can be calculated with the dry unit mass of inclusion $\rho_{s-in} = 2.68 \text{ Mg/m}^3$ (Trinh, 2011). It should be noted that the fines in all samples were kept at the same state defined by the two compaction parameters ($w_{opt-f} = 13.7\%$; $\rho_{max-f} = 1.82 \text{ Mg/m}^3$) (Wang et al. 2017; Wang et al. 2018a; Wang et al. 2018b). The optimum water content was selected for the fines in order to reach the maximum compaction dry density representing the compact state in the field condition (Trinh et al. 2012; Duong et al. 2013; Duong et al. 2016; Lamas-Lopez 2016). The mass of the fines and the water can be obtained accordingly.

For sample preparation, firstly, water was added into the fines to obtain the optimum water content $w = 13.7\%$. Then, the fines soil was stored in a hermetic container for 24 h for water homogenization. Afterwards, the homogenized fines soil was thoroughly mixed with the inclusions previously washed and dried. Finally, the mixed soil was dynamically compacted in a mould in three layers to reach the dimensions of diameter $D = 100 \text{ mm}$ and height $H = 200 \text{ mm}$. It should be noted that under a given compaction energy, the dry density of the fines varies with the change of inclusion content (Houston and Walsh 1993; Torrey and Donaghe 1994). In this study, in order to control the dry densities of the fines in all samples at the same value, higher compaction energies were applied for higher inclusion content. As a result, higher global dry densities were obtained with higher inclusion content, as shown in Table 3.

Monotonic triaxial drained tests were performed at three confining pressures ($\sigma_3 = 30 \text{ kPa}$, 60 kPa and 120 kPa). Note that no saturation procedure was applied and the sample

water content was kept constant during a test. The shear tests were carried out at a rate of 0.5 mm/min and ended after a peak deviator stress appeared (for samples with large f_v values) or after an axial strain $\varepsilon_l = 15\%$ was reached (for samples with small f_v values). Note also that for $C_u = 2.01$ at $f_v = 5\%$ and 10% under $\sigma_3 = 60$ kPa, the results are not used here because of a technique problem. Detailed information of these tests is summarized in Table 3.

To investigate the soil fabric, X-ray μ CT scans were carried out on as-compacted samples. The middle part (100 mm diameter and 100 mm height) was scanned for each. The “Ultratom” device designed and constructed by RXsolutions (France) was used with its X-ray source operated at a voltage of 170 kV and 10 μ A. A voxel size of 58.4 μ m can be detected. Note that representative samples were selected for this operation (see Table 3).

Experimental results

Changes of shear behaviour with f_v

The variations of deviator stress q and volumetric strain ε_v with axial strain ε_l for soils of $C_u = 1.12$ at five f_v values are presented in Fig. 4 for the three confining pressures. For the deviator stress q , as expected, a higher confining pressure led to a larger q . Under each confining pressure, the increase of maximum deviator pressure q_{\max} was relatively small with the increase of f_v from 5% to 20%. When f_v was larger than 35%, q_{\max} increased significantly with f_v . As far as the volumetric strain ε_v is concerned, as expected, the increase of σ_3 favored the contraction behavior. However, the dilatancy behavior was enhanced by the increase of f_v . Similar phenomena were observed for $C_u = 2.72$ (Wang et al. 2018a) and $C_u = 2.01$.

Fig. 5 shows the peak deviator stress q_{\max} against f_v for different confining pressures. It can be observed that for all the three C_u values the increasing trend of q_{\max} followed a bi-linear pattern with the distinct slopes for $f_v \leq 20\%$ and for $f_v \geq 35\%$. Moreover, a characteristic volumetric inclusion content $f_{v\text{-}cha}$ could be identified at the intersection point of the two fitting lines. It could be suspected that when $f_v \leq f_{v\text{-}cha}$ the soil fabric was controlled by a fine-fine contact structure, while when $f_v \geq f_{v\text{-}cha}$ the soil fabric was controlled by a grain-grain contact structure.

To verify this point, the 3D inclusion distributions in the as-compacted samples with different f_v values were determined based on the 2D slices obtained via X-ray μ CT scans, using ImageJ software (version 1.6.0_24, 2013, U.S. National Institutes of Health, Bethesda, Maryland). The procedures of histogram thresholding and outlier removal were applied on the 2D slices to eliminate the pixels representing the fines (diameter < 2 mm). Then, only inclusion grains were retained. The 3D structures of the inclusions were established by stacking all the processed slices. Fig. 6 shows the case of $C_u = 1.12$. It can be observed that when f_v was smaller than $f_{v\text{-}cha}$ (5% and 20%), the inclusion grains were floated in the fines matrix. On the contrary, when f_v was larger than $f_{v\text{-}cha}$ (35% and 45%), most of the inclusions were in contact with each other and constituted the soil skeleton. For the sample with $C_u = 2.72$, Wang et al. (2018a) also observed these two distinct soil fabrics.

To further clarify this aspect, quantitative characterization of the inclusion contacts was conducted by determining the average coordination number N_c . Twenty 2D cross section

slices were used for this purpose. The coordination number N_{ci} for a certain inclusion grain was defined as the total number of its neighboring grains (Jouannot-Chesney et al. 2006). For each slice, N_c was calculated by averaging the coordination number of all the inclusion grains:

$$N_c = \sum N_{ci} / Q \quad (2)$$

where N_{ci} is the coordination number of each inclusion grain; Q is the total number of the inclusion grains in a slice.

The obtained coordination numbers for $C_u = 2.01$ and 1.12 are shown in Fig. 7 as a function of f_v , along with those determined by Wang et al. (2018b) for $C_u = 2.72$. It can be observed that N_c varied in a narrow range. At each C_u value, N_c increased with increasing f_v and a parabolic function could be used to well describe this increasing trend. Furthermore, the N_c values were small and they were almost the same for f_v ranging from 5% to 20% (smaller than f_{v-cha}), indicating that in this range the inclusion grains were rarely in contact and were dispersed in the fines matrix. However, when f_v reached 35% (larger than f_{v-cha}), the N_c value increased drastically, suggesting that the contacts between the grains were well developed and the grain-grain contact structure was formed in this f_v range.

Effect of C_u on the characteristic volumetric inclusion content f_{v-cha}

From Fig. 5 it can be observed that the volumetric inclusion content f_{v-cha} shifted rightwards with the decrease of C_u : the f_{v-cha} values are 27.0%, 28.8% and 30.5% for $C_u = 2.72$, 2.01 and 1.12, respectively. This suggests that for a smaller C_u , more inclusions were needed to form a grain-grain contact structure. This phenomenon can be explained as follows: as shown in Fig.

7, the data of smaller C_u values lay below those of larger C_u values, indicating that less contacts were developed at smaller C_u value. To some extent, f_{v-cha} could be regarded as a value at which a certain number of contacts was reached. Thereby, with the decrease of C_u , the grains number and the contacts number were both expected to decrease. As a result, more grains were needed to form the grains skeleton, leading to a larger f_{v-cha} .

Changes of shear behavior with C_u in the case of grain-grain contact structure

To study the effect of C_u in the case of grain-grain contact structure, the samples of $f_v = 35\%$ sheared under $\sigma_3 = 60$ kPa and 120 kPa were considered (Fig. 8). It can be observed that the q_{max} of smaller C_u was larger. For $f_v = 35\%$ under $\sigma_3 = 30$ kPa, and for $f_v = 45\%$ under $\sigma_3 = 30$ kPa, 60 kPa and 120 kPa, the similar phenomenon was observed, which could be explained as follows: as the maximum grain diameters for the three C_u values were fixed, equal to 20 mm (Fig. 3), a smaller C_u (more uniform pattern) implied more large inclusions. As it was harder for the large inclusions to rearrange during shear, a larger q_{max} can be expected. This mechanism can be termed as “large or small” of the inclusion in terms of size. The study of Oda et al. (1982) on gravel soils also showed that the difficulty of rearrangement of gravel grains led to a larger shear strength. Regarding the volumetric strain ε_v , a smaller C_u gave rise to a larger dilatancy. This can also be explained by the more large inclusions involved in the case of smaller C_u , which favored the dilatancy.

Changes of shear behavior with C_u in the case of fine-fine contact structure

For the fine-fine contact structure where the inclusions were dispersed in the fines matrix ($f_v = 5\%$ and 10%), it appears that on the whole q_{max} decreased with the decrease of C_u under $\sigma_3 = 60$ kPa (Fig. 9b with 2 C_u values) and $\sigma_3 = 120$ kPa (Fig. 9c with 3 C_u values). However, the changes of q_{max} with C_u under $\sigma_3 = 30$ kPa does not appear significant (Fig. 9a with 3 C_u values). One possible explanation is that q_{max} reflects the friction at failure, and this friction is basically governed by both the soil property (mainly the amount of coarse grains involved in the friction process) and the confining pressure (corresponding to the normal stress in the friction process). Perhaps 30 kPa confining pressure was not high enough to reveal the C_u effect on q_{max} . The decreasing trend of q_{max} with decreasing C_u in the cases of 60 kPa and 120 kPa could be explained by the fact that the amount of inclusion grains decreased with the decreasing C_u and therefore less inclusion grains were expected to be involved in the friction process (in the shear band zone for instance), giving rise to a smaller q_{max} . The 3D views of the inclusions in the sample of $f_v = 5\%$ with $C_u = 2.01$ and $C_u = 1.12$ came to support this reasoning (Fig. 10). This mechanism can be termed as “more or less” of the inclusions in terms of amount.

As far as the volumetric strain ε_v is concerned, it can be observed that when C_u increased, the dilatancy became more significant. This is because larger amount of grains was involved with larger C_u , which increased the grain-grain contacts, leading to larger dilatancy.

At $f_v = 20\%$, the results were a little different from those at $f_v = 5\%$ and 10% . Under $\sigma_3 = 60$ kPa and 120 kPa (Fig. 11a; Fig. 11b), different C_u values gave similar q_{\max} and similar ε_v . This could be explained by the fact that in that case the inclusions started to be in contact with each other without developing a well-defined skeleton. Thereby, both mechanisms of “large or small” and “more or less” were involved. As the effects of the two mechanisms were opposite, the global mechanical response of soil showed independent feature with respect to C_u .

Variation of Young’s modulus with C_u

The Young’s modulus E_0 characterizes the stiffness of the track-bed materials (Lamas-Lopez 2016) and it is often used in analysing the dynamic response of the rail platform (Zhang et al. 2016). The results obtained allowed the effect of C_u of inclusions on this modulus to be assessed. For simplify, Young’s modulus E_0 was defined here as the ratio of q to ε_1 at $\varepsilon_1 = 1\%$. The variations of E_0 with C_u are depicted in Fig. 12. It appears that when f_v increased, E_0 increased and the influence of C_u became more pronounced. At each f_v value, a smaller C_u led to a larger E_0 , which could also be explained by relatively more large inclusions.

Variation of Poisson’s ratio and dilatancy angle with C_u

Based on the volumetric strain-axial strain curves, Poisson’s ratio ν and the dilatancy angle ψ can be determined following the equations proposed by Vermeer and Borst (1984):

$$\nu = \frac{1 - k_C}{2} \quad (2)$$

$$\sin \psi = \frac{k_D}{-2 + k_D} \quad (3)$$

where k_c and k_D are the slopes of the contraction phase and dilatancy phase of the curves, respectively (see Fig. 13).

Fig. 14 depicts the variations of ν with C_u at different f_v values. It is observed that at $f_v = 5\%$ and 10% (fine-fine contact structures), ν decreased with the decrease of C_u , indicating that the lateral strain was decreased when more grains were dispersed in the fines matrix. Note that though $f_v = 20\%$ was categorized in the group of fine-fine contact fabric, the effect of C_u on Poisson's ratio followed the same pattern of grain-grain contact fabric: the smaller the C_u value, the larger the ν . In this case, the mechanism of "large or small" of the inclusions might play a dominant role. This increase of ν was normal since at a given axial strain the lateral strain was expected to be larger when larger grains are involved.

The variations of dilation angle ψ with C_u are shown in Fig. 15. For the samples with small f_v values (e.g. $f_v = 5\%$) and large confining pressures, it appears difficult to establish any correlations. In addition, the grain-grain contact structure corresponding to smaller C_u values led to a larger ψ , while in the case of fine-fine contact structure, ψ seems to decrease with the decrease of C_u .

Variations of cohesion and friction angle with C_u

The values of friction angle ϕ and cohesion c are determined using the following equations

(Wood 1990):

$$\sin \phi = \frac{3M}{6+M} \quad (4)$$

$$c = \frac{S(3-\sin \phi)}{6 \cos \phi} \quad (5)$$

where M and S are the slope and intercept of the failure line in p - q plane. It is worth noting that in this study, the saturation degrees of all samples at different f_v values were strictly the same (see Table 3), because all water was expected to be contained in the fines soils and both water content and dry density were kept the same for all samples. As suction was developed inside the fines, the initial suctions of all samples were also the same. The obtained values of friction angle ϕ and cohesion c include the contribution of this suction. But of course, suction would change during shearing and this was ignored in the analysis.

Fig. 16 shows the variations of cohesion with C_u . On the whole, the cohesion decreased with increasing C_u . A possible explanation is as follows: when C_u increased, more small grains were involved and thus more grain-grain contacts were created. As a result, less fine-fine contacts were expected and thus lower cohesion was obtained.

When it comes to the friction angle (Fig. 17), for grain-grain contact structure ($f_v = 35\%$ and 45%), a smaller C_u value led to a larger friction angle. Note that the case of $f_v = 20\%$ obeyed the same rule. This can be explained by the more difficult rearrangement of grains in the case of smaller C_u (more larger grains). Oda et al. (1982) and Skinner (1969) also reported the correlation between the difficulty of grains rearrangement and the friction angle for granular materials. As opposed to the grain-grain structure, the fine-fine contact structure ($f_v = 5\%$ and 10%) exhibited a smaller friction angle at smaller C_u value. This can be attributed to the presence of less coarse grains along the shear band because the friction angle ϕ is mainly controlled by coarse grains.

Conclusions

Monotonic triaxial tests and X-ray μ CT scans were performed on a material simulating the interlayer soils, with inclusions and fines. The effect of coefficient of uniformity C_u of inclusions on the mechanical behaviors was investigated with five volumetric inclusion contents ($f_v = 5\%$, 10% , 20% , 35% and 45%). Three C_u values, 2.72, 2.01 and 1.12, were considered. The obtained results allowed the effect of C_u on the mechanical behavior to be analyzed.

For a given C_u , from the variation pattern of peak deviator stress q_{max} with the volumetric inclusion content f_v , a characteristic volumetric inclusion content f_{v-cha} was identified, defining two soil fabrics: a fine-fine contact structure and a grain-grain contact structure. The f_{v-cha} increased with the decrease of C_u because in this case more inclusions were needed to develop the grain-grain contact structure. This point was verified by the μ CT scans.

In the case of grain-grain contact structure, the number of large inclusion grains is a key parameter controlling different mechanical characteristics. The decrease of C_u was found to increase the friction angle as well as the peak deviator stress q_{max} , because more large inclusions were involved in this case and it was more difficult for large inclusions to rearrange during shearing. A larger Poisson's ratio and a larger dilatancy angle were observed at smaller C_u . This can also be explained by the involvement of more large grains in that case,

leading to a larger lateral strain at a given axial strain in the contraction phase and a larger volume change in the dilatancy phase.

By contrast, in the case of fine-fine contact structure, it is the amount of all inclusion grains that governs the overall soil behaviour. It was observed that a smaller C_u corresponding to a smaller inclusion grain quantity led to a smaller friction angle and a smaller q_{max} , due to less inclusion grains that could be expected in the shear band zone. In addition, the Poisson's ratio decreased with decreasing C_u because the horizontal restriction was expected to be weakened with a lower quantity of inclusions dispersed in the fines matrix. The dilatancy behavior was less pronounced at smaller C_u because less grain contacts were developed in case of smaller quantity of inclusions.

The variations of Young's modulus with increasing C_u were the same for the two soil fabrics: Young's modulus decreased with the increase of C_u due to relatively less grain-grain contacts. In addition, the two soil fabrics also shared the same varying pattern in terms of cohesion: the cohesion decreased with increasing C_u . This is because only the fine-fine contacts were expected to contribute to the cohesion and such contacts decrease with the increase of inclusions quantity.

The findings from this study help assess the mechanical behavior of interlayer soils with inclusions of different C_u values. It can be deduced that an interlayer soil with a large C_u value exhibits a low shear strength and thus a low mechanical performance under the effect of train loading. Therefore, if the C_u values are determined over a rail network, the

mechanical performance related to C_u can be assessed over such a whole network. However, it is worth noting that the test conditions considered in this study are quite limited (triaxial tests on a mixture at a fixed water content and with scale-down inclusions). More comprehensive studies are needed to approach the complex field conditions.

Acknowledgements

The support from the Chinese Scholar Council (CSC) and the French Railway Company (SNCF) are greatly acknowledged.

NOTATION

C_u	coefficient of uniformity
d_{max}	maximum grain diameter of micro-ballast
d_{60}	grain diameter at 60% passing
d_{10}	grain diameter at 10% passing
c	cohesion
D	diameter of sample
e	void ratio of sample
E_0	Young's modulus
f_{v-cha}	characteristic volumetric inclusion content
f_v	volumetric inclusion content
H	height of sample
I_p	plasticity index
M	slope of the failure line in p - q plane
k_C	slope of volumetric strain versus axial strain in the contraction phase
k_D	slope of volumetric strain versus axial strain in the dilatancy phase
N_{ci}	coordination number for a certain inclusion grain in a slice
N_c	average coordination number of inclusion grains in a slice

Q	total number of inclusion grains in a slice
q	deviator stress
q_{\max}	maximum deviator stress
S	intercept of the failure line in p - q plane
S_r	saturation degree of sample
V_{in}	volume of total inclusion grains
V_{total}	volume of total sample
V_{fines}	volume of fines
w	water content of fines
w_L	liquid limit
w_{opt-f}	optimum water content of fines
ρ_d	dry unit mass of sample
ρ_{s-in}	dry unit mass of inclusion grains
ρ_{max-f}	maximum dry unit mass of fines
σ_3	confining pressure
ε_l	axial strain
ε_v	volumetric strain
ν	Poisson's ratio
ψ	dilatancy angle
φ	friction angle

References

- Cui Y.J., Duong T.V., Tang A.M., Dupla J.C., Calon N., Robinet A., 2013. Investigation of the hydro-mechanical behavior of fouled ballast. *J. Zhejiang Univ-Sci. A (Appl. Phys. Eng.)* 14 (4), 244-255.
- Duong, T.V., Tang, A.M., Cui, Y.J., Trinh, V.N., Dupla, J.C., Calon, N., Canou, J., Robinet, A., 2013. Effects of fines and water contents on the mechanical behavior of interlayer soil in ancient railway sub-structure. *Soils Found.* 53 (6), 868-878.
- Duong, T.V., Cui, Y.J., Tang, A.M., Dupla, J.C., Canou, J., Calon, N., Robinet, A., 2016. Effects of water and fines contents on the resilient modulus of the interlayer soil of railway substructure. *Acta Geotech.* 11 (1), 51-59.
- Fagnoul, A., Bonnechere, F., 1969. Shear strength of porphyry materials. *Proc. 7th Int. Conf. Soil Mech. Found. Eng., Mexico.*
- Houston, S. L., and Walsh, K. D., 1993. Comparison of rock correction methods for compaction of clayey soils. *J. Geotech. Eng.* 119(4): 763-778.
- Igwe, O., Sassa, K., Wang, F., 2007. The influence of grading on the shear strength of loose sands in stress-controlled ring shear tests. *Landslides.* 4: 43-51.
- Jouannot-Chesney, P., Jernot, J. P., and Lantuejoul, C., 2006. Particle determination of the coordination number in granular media. *Image Anal Stereol.* 25, 55-61.

Kokusho, T., Hara, T., Hiraoka, R., 2004. Undrained shear strength of Granular Soils with

Different Particle Gradations. *Journal of Geotechnical and Geoenvironmental*

Engineering. 130 (6): 621-9.

Lamas-Lopez, F., 2016. Field and laboratory investigation on the dynamic behaviour of

conventional railway track-bed materials in the context of traffic upgrade (PhD Thesis).

Ecole Nationale des Ponts et Chaussées, Université Paris-Est.

Lowe, J., 1964. Shear strength of coarse embankment dam materials. *Proc. 8th Int. Congr.*

Large Dams 3, Edimbourg, UK.

Menq, F.Y. 2003. *Dynamic Properties of Sandy and Gravelly Soils*. PhD Thesis, The

University of Texas at Austin.

Monkul, M.M., Etmnan, E., Senol, A., 2016. Influence of coefficient of uniformity and base

sand gradation on static liquefaction of loose sands with silt. *Soil Dynamics and*

Earthquake Engineering. 89 : 185-197.

Nitchiporovitch, A.A., 1969. Shearing strength of coarse shell materials. *Proc. 7th Int. Conf.*

Soil Mech. Found. Eng., Mexico.

Oda, M., Konishi, J., Nasser, N.S., 1982. Experimental micromechanical evaluation of

strength of granular materials : effects of particle rolling. *Mechanics of Materials*. 1982 :

269-283.

- Pedro, L., 2004. De l'étude du comportement mécanique de sols hétérogènes modèles à son application au cas des sols naturels (PhD Thesis). Ecole Nationale des Ponts et Chaussées.
- Seif El Dine, B., Dupla, J.C., Frank, R., Canou, J., Kazan, Y., 2010. Mechanical characterization of matrix coarse-grained soils with a large-sized triaxial device. *Can. Geotech. J.* 47, 425-438.
- Skinner, A.E., 1969. A note on the influence of interparticle friction on the shear strength of a random assembly of spherical particles. *Geotechnique*. 19, 150.
- Torrey, V. H., and Donaghe, R. T., 1994. Compaction control of earth-rock mixtures: a new approach. *Geotech. Test. J.* 17(3): 371-386.
- Trinh, V.N., 2011. Comportement hydromécanique des matériaux constitutifs de plateformes ferroviaires anciennes (PhD Thesis). Ecole Nationale des Ponts et Chaussées, Université Paris-Est.
- Trinh, V.N., Tang, A.M., Cui, Y.J., Dupla, J.C., Canou, J., Calon, N., Lambert, L., Robinet, A., Schoen, O., 2012. Mechanical characterisation of the fouled ballast in ancient railway track sub-structure by large-scale triaxial tests. *Soils Found.* 52 (3), 511-523.
- Vermeer, P.A., de Borst, R., 1984. Non-Associated Plasticity for Soils, Concrete and Rock. *Heron* 29 (3), 1-64.
- Wang, H. L., Cui, Y. J., Lamas-Lopez, F., Dupla, J. C., Canou, J., Calon, N., Saussine, G., Aïmediou, P., Chen, R. P., 2017. Effects of inclusion contents on resilient modulus and

damping ratio of unsaturated track-bed materials. *Canadian Geotechnical Journal*. 54, 1672-1681.

Wang, H. L., Cui, Y. J., Lamas-Lopez, F., Calon, N., Saussine, G., Dupla, J. C., Canou, J., Aimedieu, P., Chen, R. P., 2018a. Investigation on the mechanical behavior of track-bed materials at various contents of coarse grains. *Construction and Building Materials journal*. 164, 228-237.

Wang, H. L., Cui, Y. J., Lamas-Lopez, F., Dupla, J. C., Canou, J., Calon, N., Saussine, G., Aimedieu, P., Chen, R. P., 2018b. Permanent deformation of track-bed materials at various inclusion contents under large number of loading cycles. *Journal of Geotechnical and Geoenvironmental Engineering*. 144(8): 04018044.

Wichtmann, T. and Triantafyllidis, T., 2009. Influence of the Grain-Size Distribution Curve of Quartz Sand on the Small Strain Shear Modulus G_{max} . *Journal of Geotechnical and Geoenvironmental Engineering*. 135(10): 1404-1418.

Wood, D. M., 1990. *Soil behavior and critical state soil mechanics*. Cambridge University Press, Cambridge.

Zhang, T.W., Cui, Y.J., Lamas-Lopez, F., Calon, N., Costa d'Aguiar, S. 2016. Modelling stress distribution in substructure of French conventional railway tracks. *Construction and Building Materials* 116: 326–334.

List of Tables

Table 1. Proportions of the nine commercial soils

Table 2. Basic properties of micro-ballast with 3 different C_u values

Table 3. Experimental program

Table 1. Proportions of the nine commercial soils

Soil Symbol	Mass proportion (%)	Grain size range (mm)
Bentonite	6.7	0.001 - 0.01 (20% of the particles)
Speswhite	23.3	0.0003 - 0.01 (80% of the particles)
C-10	20.0	0.0009 - 0.25
C-4	16.7	0.0009 - 0.50
HN 34	3.3	0.063 - 0.50
HN 31	3.3	0.16 - 0.63
HN 0.4-0.8	6.7	0.25 - 1
HN 0.6-1.6	6.7	0.32 - 2
HN 1-2.5	13.3	0.32 - 3.20

Table 2. Basic properties of micro-ballast with 3 different C_u values

Sample name	Proportions of the constitutive soils (%)			C_u (designed)	C_u (measured)
	G10-20	G4-10	HN2-4		
S1	34	58	8	2.72	2.67
S2	85	15	0	2.01	2.00
S3	16-20 mm	0	0	1.12	1.12

Table 3. Experimental program

f_v (%)	ρ_d (Mg/m ³)	e	S_r (%)	C_u	Monotonic Triaxial Test	μ CT Test
					σ_3 (kPa)	
5	1.86	0.437	78	2.72	30, 60, 120	√
				2.01	30, 120	√
				1.12	30, 60, 120	√
10	1.91	0.404	78	2.72	30, 60, 120	√
				2.01	30, 120	—
				1.12	30, 60, 120	—
20	1.99	0.343	78	2.72	30, 60, 120	√
				2.01	30, 60, 120	—
				1.12	30, 60, 120	√
35	2.12	0.262	78	2.72	30, 60, 120	√
				2.01	30, 60, 120	—
				1.12	30, 60, 120	√
45	2.21	0.212	78	2.72	30, 60, 120	√
				2.01	30, 60, 120	√
				1.12	30, 60, 120	√

Note: ρ_d , e and S_r are the sample' dry density, void ratio and degree of saturation, respectively.

List of Figures

Fig. 1. Grain size distributions of fines (modified from Wang et al. 2018a)

Fig. 2. Grain size distributions of the in-situ ballast, the micro-ballast and the three constitutive materials (modified from Wang et al. 2018a)

Fig. 3. Grain size distributions of micro-ballast materials S1, S2 and S3

Fig. 4. Shear behavior of soils with $C_u = 1.12$ and different f_v values under: (a) $\sigma_3 = 30$ kPa; (b) $\sigma_3 = 60$ kPa; (c) $\sigma_3 = 120$ kPa

Fig. 5. Variations of peak deviator stress with f_v under different σ_3 values for: (a) $C_u = 2.72$; (b) $C_u = 2.01$; (c) $C_u = 1.12$

Fig. 6. Three-dimensional views of the inclusion distributions in as-compacted samples

Fig. 7. Comparison of coordination number of the samples with different C_u values

Fig. 8. Shear behavior of soils at $f_v = 35\%$ and 3 different C_u values under : (a) $\sigma_3 = 60$ kPa; (b) $\sigma_3 = 120$ kPa

Fig. 9. Shear behavior of soils at $f_v = 5\%$ and 10% and 3 different C_u values under: (a) $\sigma_3 = 30$ kPa; (b) $\sigma_3 = 60$ kPa; (c) $\sigma_3 = 120$ kPa

Fig. 10. 3D views of the inclusion distributions in samples at $f_v = 5\%$ and (a) $C_u = 2.01$, (b) $C_u = 1.12$

Fig. 11. Shear behavior of soils at $f_v = 20\%$ and 3 different C_u values under: (a) $\sigma_3 = 60$ kPa; (b) $\sigma_3 = 120$ kPa

Fig. 12. Variations of initial modulus E_0 with f_v for different C_u and σ_3 values

Fig. 13. Determination of Poisson's ratio and dilatancy angle

Fig. 14. Variations of Poisson's ratio with f_v for different C_u and σ_3 values

Fig. 15. Variations of dilation angle with f_v for different C_u and σ_3 values

Fig. 16. Variations of cohesion with f_v for different C_u values

Fig. 17. Variations of friction angle with f_v for different C_u values

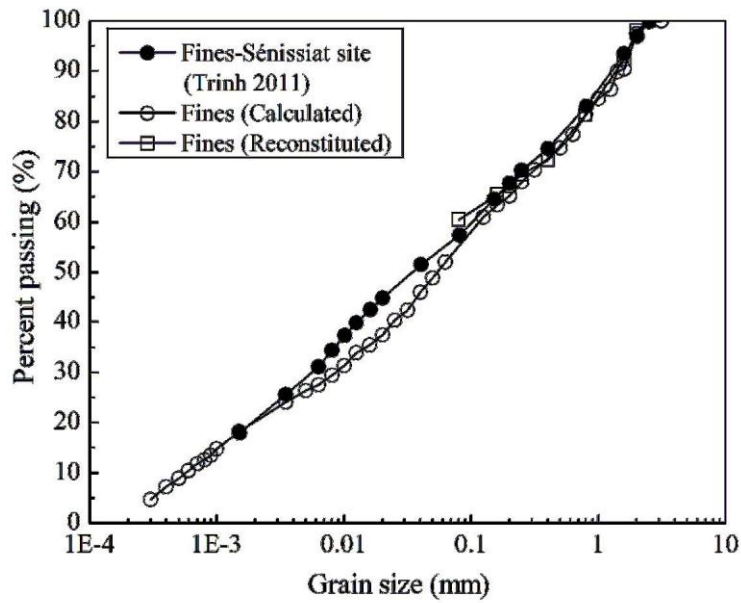


Fig. 1

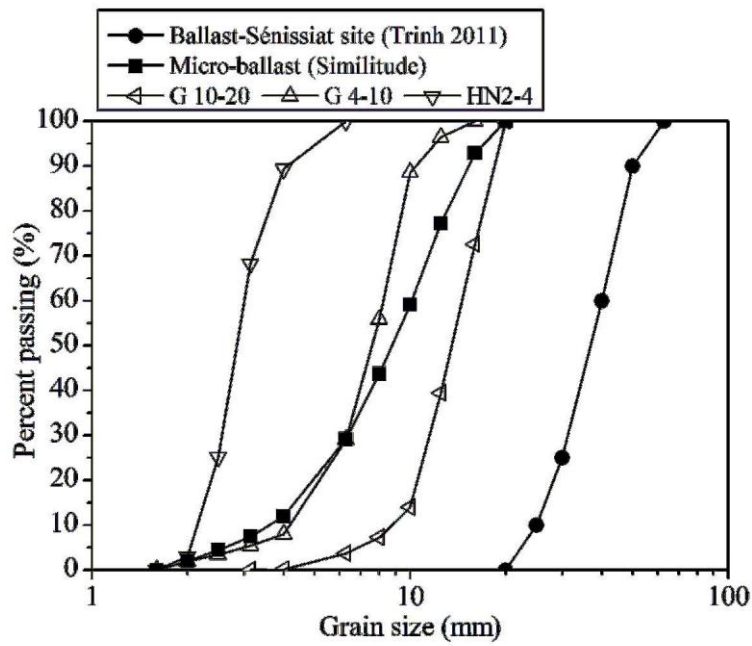


Fig. 2

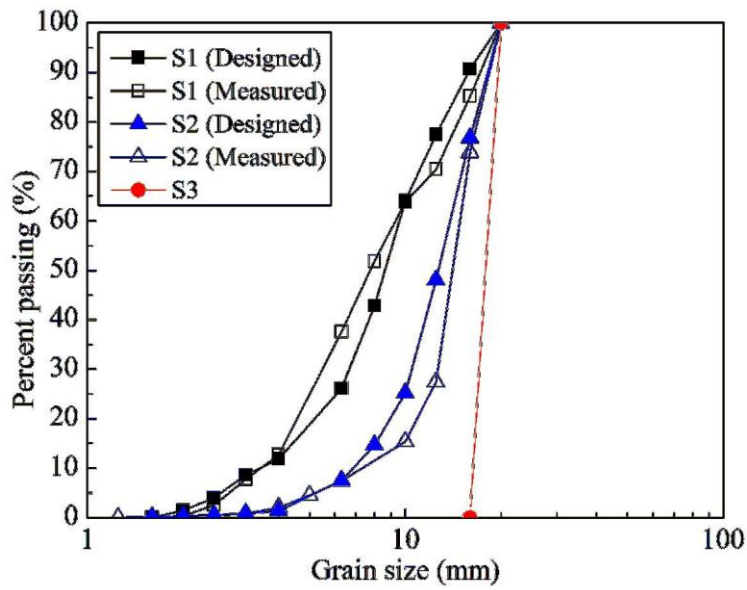


Fig. 3

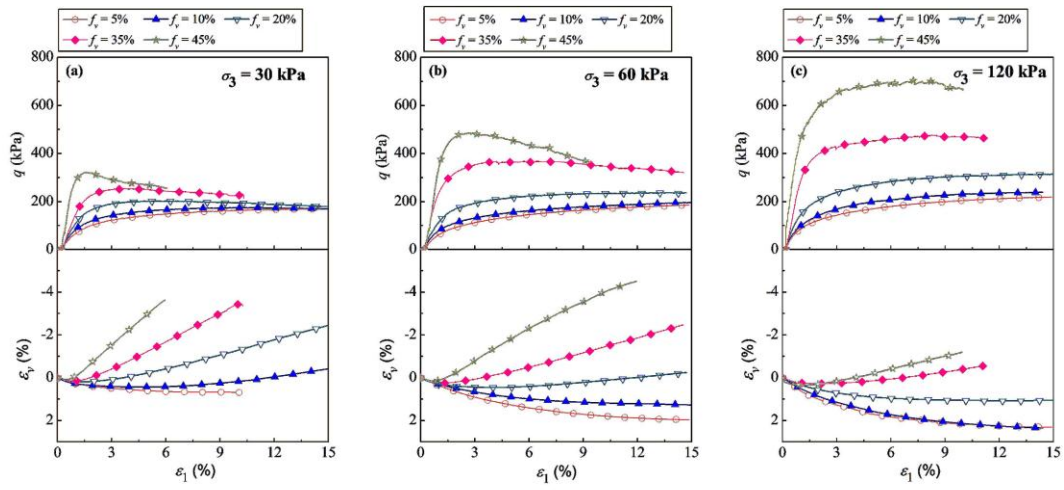


Fig. 4

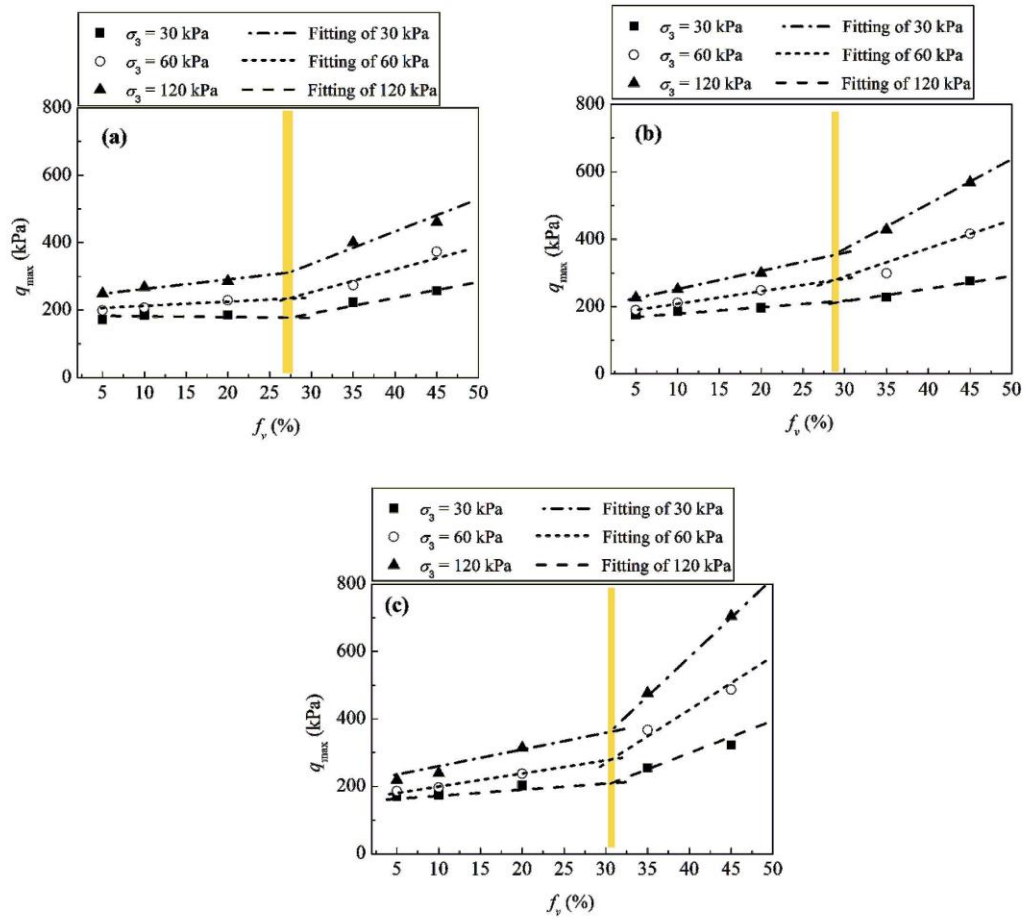


Fig. 5

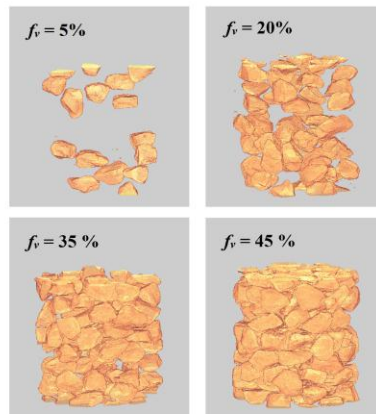


Fig. 6

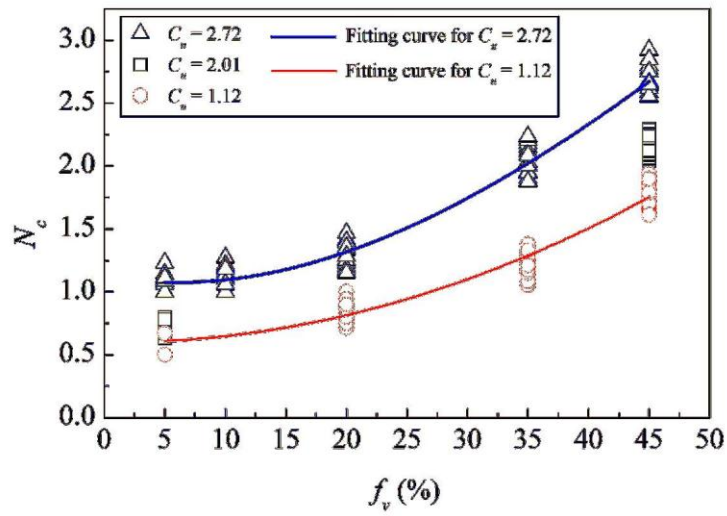


Fig. 7

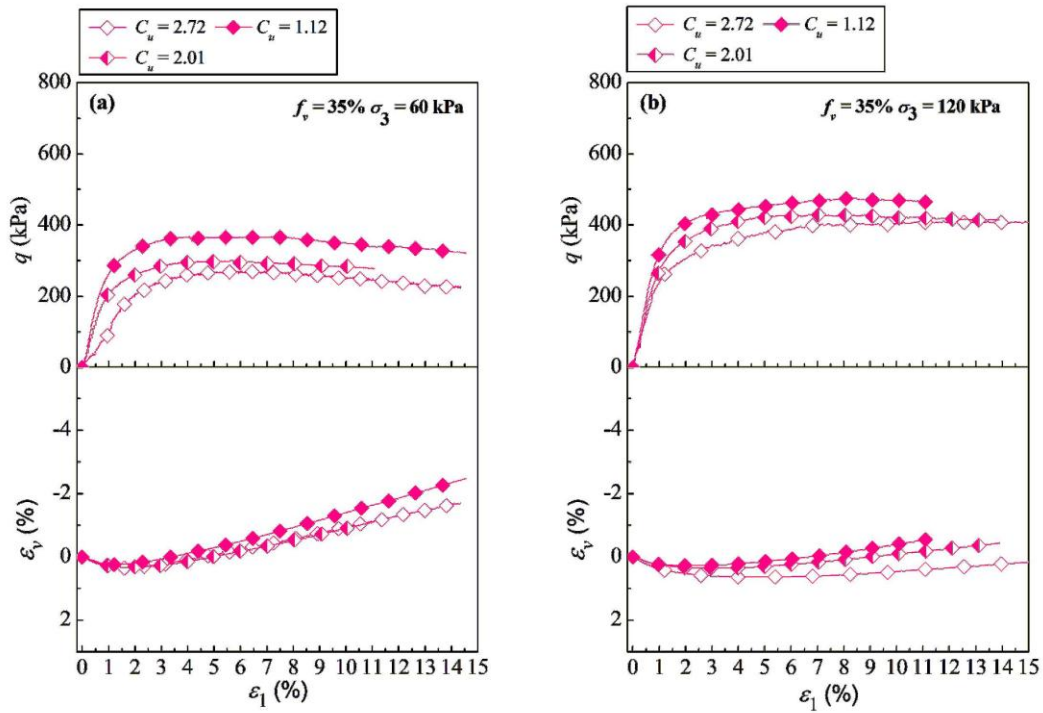


Fig. 8

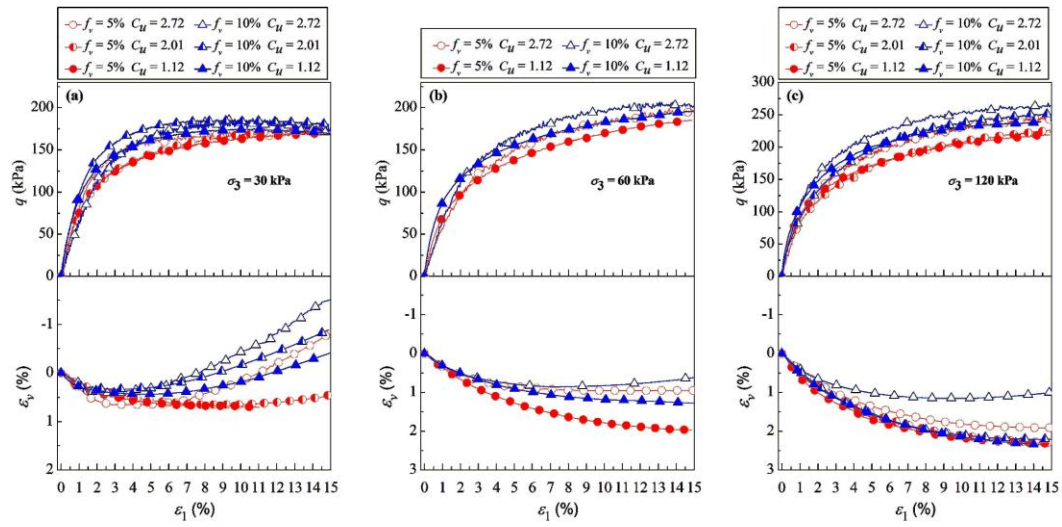


Fig. 9

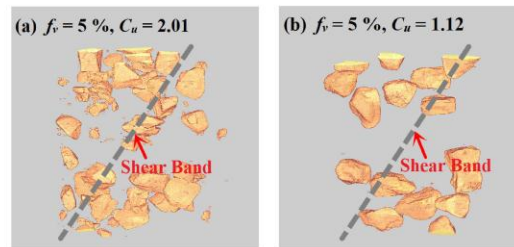


Fig. 10

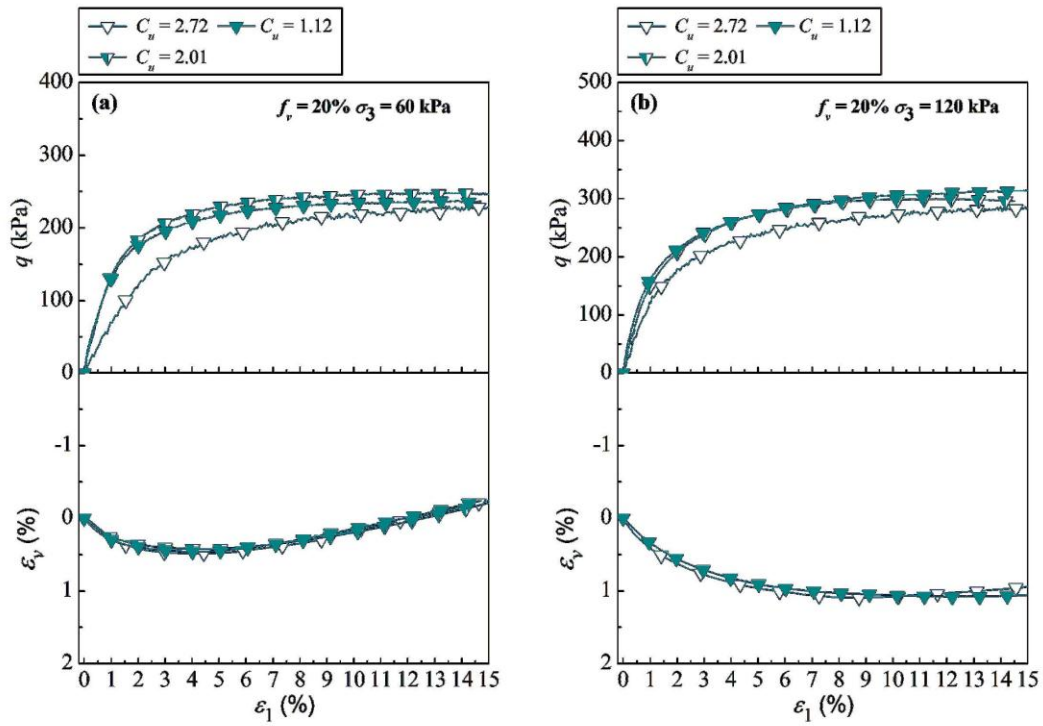


Fig. 11

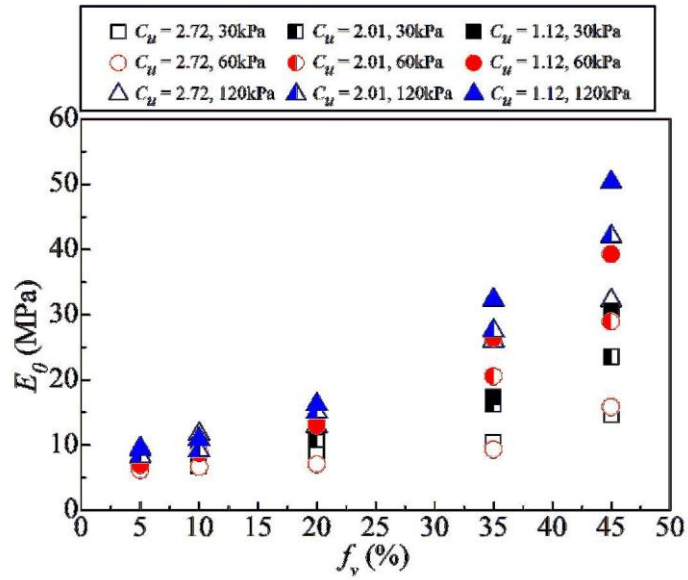


Fig. 12

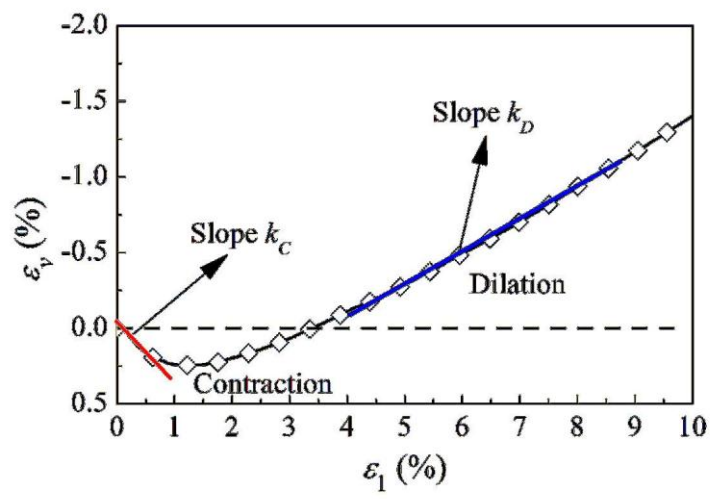


Fig. 13

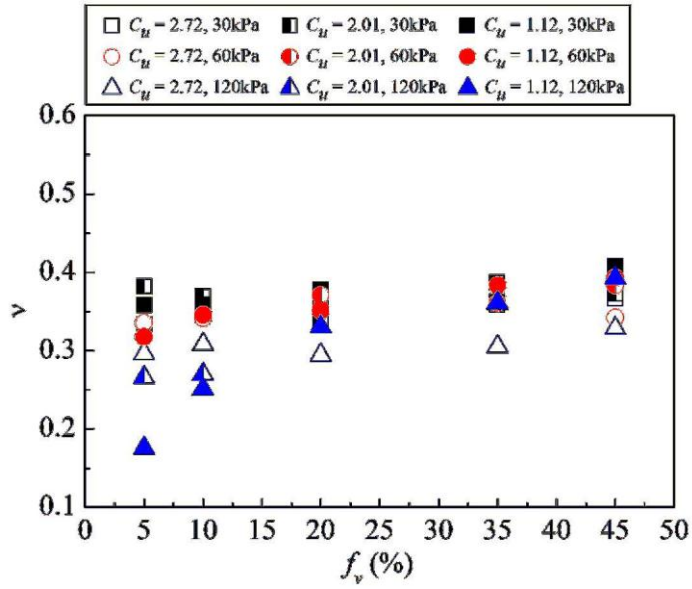


Fig. 14

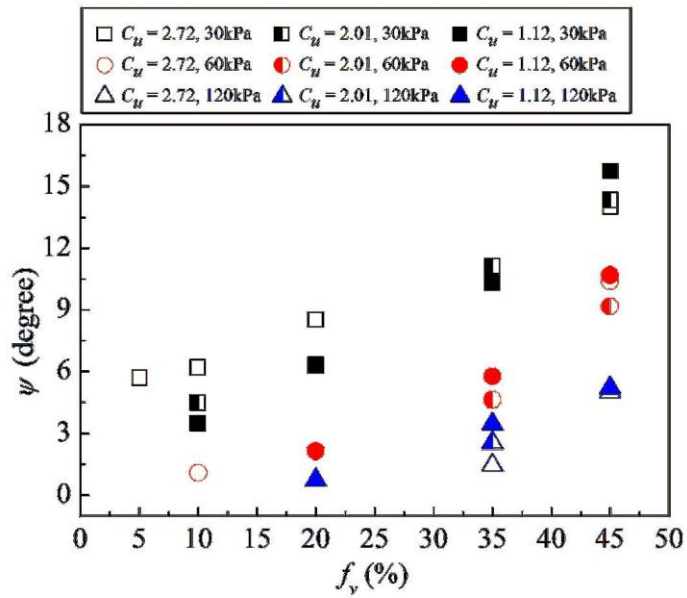


Fig. 15

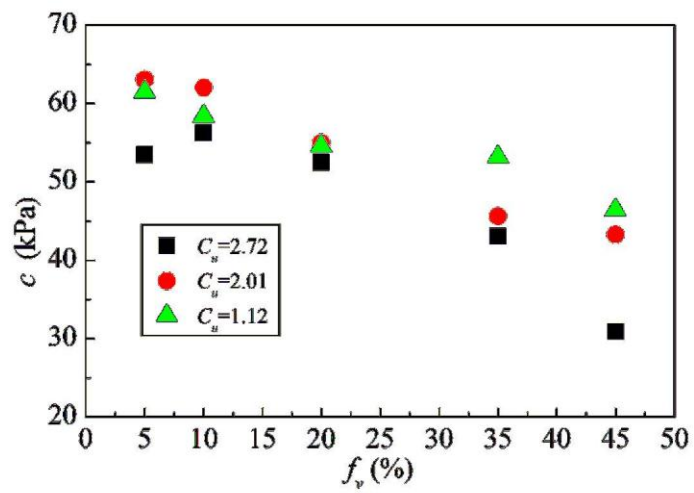


Fig. 16

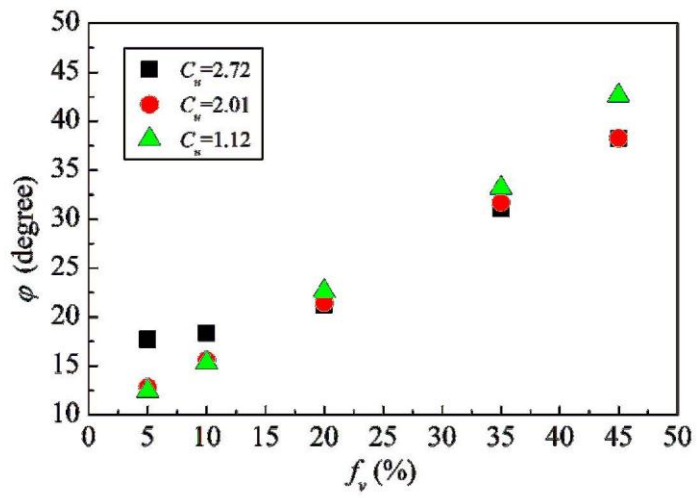


Fig. 17